WWW.IJRPR.COM

International Journal of Research Publication and Reviews

Journal homepage: www.ijrpr.com ISSN 2582-7421

Room Temperature Ionic Liquid Assisted Synthesis of Manganese Nanocomposite: PANI-$MnFe_2O_4$-CITAB for Magnetic Semiconductor via *in situ* Polymerization Method

Ibrahim Isah Fagge [1],Sabiu Shafiu [2], Sani Saminu Bala [3]

[1,2,3] Department of Chemistry, Faculty of Science, Kano University of Science and Technology, Wudil, Nigeria

DOI: https://doi.org/10.55248/gengpi.2022.3.9.8

ABSTRACT

Cetyltrimethylammoniumbromide (CTAB) and 1-butyl-3-methylimidazolium triflоromethanesulfate were used as surfactant and ionic liquid respectively for the synthesis of PANI-$MnFe_2O_4$-CITAB nanocomposite via in situ Polymerization method. The average crystalline value of the synthesized compound was determined using X-ray diffraction machine which was around 26nm. The magnetic, spectroscopic and morphological properties of the composite were determined using Vibrating Sample Magnetometry (VSM), Fourier Transform Infrared Spectroscopy (FT-IR) and Transmission Electron Microscope (TEM) respectively. From the magnetic investigation it revealed that the magnetic properties such as saturation magnetization, coercivity and remanence magnetization all increases with decrease in temperature. The electrical properties of the compound such as conductivity and permittivity were also investigated using impedance spectroscopy at the range of up to 3 MHz frequency and 20 to 120^o C temperature.

KEYWORDS; Nanocomposite; semiconductor; magnetic; permittivity; permittivity

1. INTRODUCTION

Among the magnetic nanocompound, manganese ferrite ($MnFe_2O_4$) is a kind of such spinel ferrite material with a partial inverse spinel structure and remarkable properties. It has moderate saturation magnetization of about 80 emu/g and small HC (smaller than 100 Oe). The compound has shown application in the field of electronics, microwave devices, magnetic storage, etc. [1,7]. In medicinal and biomedical technology, $MnFe_2O_4$ nanoparticle can be used in magnetic resonance imaging (MRI), biosensor and hyperthermia microwave devices, magnetic storage, etc. [5].

The observed synergetic behavior by many authors between the polymeric and inorganic material in many applications such as sensors, imaging agents, electromagnetic interference, shielding storage media, and catalysis in biotechnology and microelectronics, opened a new page in the world of nanotechnology for the synthesis of nano inorganic/polymer composite material [2,9].

Polyaniline (PANI) is a conducting polymer with a stable band gap of 2.8 eV showing strong absorption for visible light that can be used in photocatalysis (Mornet et al; 2006), doped form of it has an optical band gap 2.21 eV and room electrical conductivity (σAC = 3.12 $\times$ 10^{-2}cm^{-1}) (Yakuphanoglu et al; 2006). Due to its ease of preparation, low cost, light weight, good electronic, optical properties its stability in air as well as the solubility in so many solvents make it useful in different aspect in modern technology such as biosensors, corrosion devices, microwave absorption, optoelectronic device, electrochromic displays and chemical sensors (MacDiarmid et al; 1987). Conjugation in polymers like polyaniline make it to have excellent thermal stability and good oxidation resistance, which make it suitable as electrode materials in electro-catalysis in solar energy conversion (Bereznev*et al*; 2006). Having an electrical conductivity of (σAC = 3.12 $\times$ 10^{-2}cm^{-1}), PANI is used as hole injection layers in flexible light emitting diodes [3,8].

Cetyl trimethylammonium bromide (CTAB) is considered as very good cationic detergent, it is a watersoluble compound and widely used in the synthesis of crystalline nanocompound. As a surfactant, it may act as a surface coating to the resulting nanomaterials so as to prevent it from agglomeration being magnetic in nature, thereby controlling the size of the nano materials [19].

For this research, we shall describe a facile and eco-friendly method of synthesizing PANI–$MnFe_2O_4$-CTAB nanocomposites assisted by 1-butyl-3-methyl-imidazolium tri- fluoromethane sulfonate as ionic liquid (RTILs). The effect of the imidazolium-based ionic liquid on the properties of the synthesized compound was fully investigated. The synthetic method can be regards as green chemistry due to its reduced pollution effect during the synthesis, because both water and 1-butyl-3-methyl-imidazolium trifluoromethane sulfonate are generally considered as room temperature ionic liquid (RTILs), which are environmentally friendly solvents [4,11] were used.

2. METHODOLOGY

2.1 Reagents

Iron (III) chloride hexahydrate (98 %), $FeCl_3 \cdot 6H_2O$ (98 %), manganese (II) chloride (98 %), $MnCl_2 \cdot 4H_2O$, aniline monomer (≥99.5 %), Cetyl trimethylammonium bromide (CTAB) (99 %), hydrochloric acid(HCl) and Sodium hyroxide (NaOH) were all obtained from Merck and 1-butyl-3-methyl-imidazolium trifluoro methane sulfonate (RTILs) (99 %) from Alfa–Aesar. They were used as-received, without further purification.

2.2 Instrumentations

VSM measurements were conducted using vibrating sample magnetometer (LDJ Electronics Inc., Model 9600) and magnetization measurements were carried out in an external field up to 50 kOe at room temperature. Fourier transform infrared (FT-IR) spectra of the samples were recorded with a Perkin Elmer BX FT-IR infrared spectrometer in the range of 4000–400 cm−1.

X-ray powder diffraction (XRD) analysis was performed on the sample by Rigaku Smart Lab operated at 40 kV and 35 mA using Cu Kα radiation (λ=1.54059 Å). The electrical conductivities of the PANI–MnFe2O4-CTAB nanocomposite in RTILs were observed in the temperature range of 20–120 oC at a heating rate of 10 oC/s. The sample was used in the form of circular pellets of 13 mm diameter and 3 mm thickness. The pellets (both nanocomposite and pristine) were sandwiched between gold electrodes.

However, the conductivities of the as prepared compound were measured using Novocontrol dielectric impedance analyzer in the frequency range 1 to 3 MHz, respectively, under control temperature of 100 and 250 oC. Transmission electron microscopy (TEM) analysis was performed using FEI Tecnai G2 Sphera microscope. The thermal stability of the nanocomposite was determined by thermo-gravimetric analysis (TGA, Perkin Elmer Instruments model, STA 6000). The TGA thermograms were recorded using 5 mg of powder sample at a heating rate of 10 oC/min in the temperature range of 30 to 750 oC under inert atmosphere.

2.3 Procedure

2.3.1 Synthesis of manganese ferrite, $MnFe_2O_4$ Nanoparticles

The magnetic component ($MnFe_2O_4$) was synthesized using novel hydrothermal synthetic method using Cetyl trimethylammonium bromide (CTAB) as surfactant. A measured amount $MnCl_2 \cdot 6H_2O$ and $FeCl_3 \cdot 6H_2O$ in the ratio of 1:2 metal precursors were dissolved in 50 ml distilled water and 0.7 g CTAB was also dissolved in 20 ml water. The two solutions were mixed and the pH was raised to pH=11 using 2 M NaOH under vigorous stirring at 80 ^oC for about 60 minutes. The obtained clear solution was transferred into 50 mL stainless steel autoclave, sealed, and put into oven heated at 180 ^oC for 12 h, it then removed cooled under laboratory temperature. Finally, the product was washed with distilled water and ethanol for several times to remove the impurities and dried in an oven at 80 ^oC for 4 h.

2.3.2 Synthesis of PANI–$MnFe_2O_4$-CTAB Nanocomposite in RTILs

1 g of the synthesized nanoparticles above and 5.0 mL 1-butyl-3- methyl-imidazolium trifluoromethane sulfonate (RTILs), were dispersed into 30 ml 0.001 M HCl solution in a three-neck round-bottomed flask fitted with ultrasonic vibration for 1 h, then 1.8 mL aniline monomer was added to the mixture, and an ultrasonic vibration was continued for another 30 min. The reaction system was then cooled in an ice bath. Under the protection with nitrogen gas, the ammonium peroxydisulfate (5 g, dissolved in 1.8 M HCl solution), which serves as an oxidant, was added drop-wise into the above mixture. The reaction was continued for 18 h at 0 ^oC.

3. RESULTS AND DISCUSSION

3.1 XRD Analysis

Fig. 1 presents the XRD pattern of PANI-$MnFe_2O_4$-CTAB nanocomposite. All of the observed diffraction peaks are indexed by the cubic structure of the magnetic $MnFe_2O_4$.

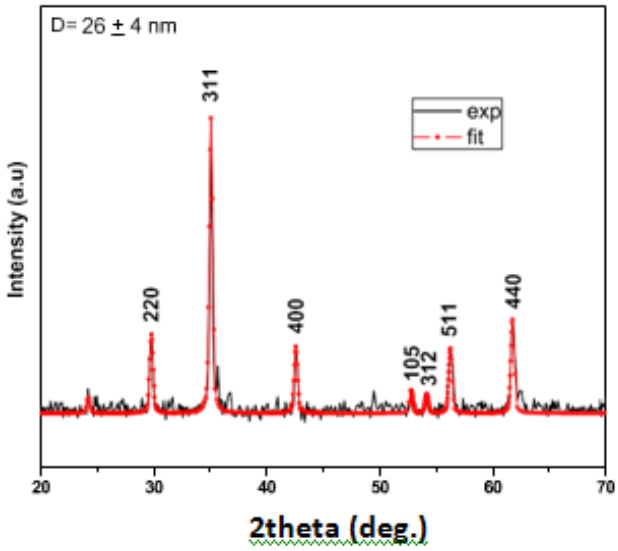

Fig.1: XRD powder pattern of PANI–$MnFe_2O_4$-CTAB nanocomposite.

A careful understanding of the broadening of the diffraction peaks clearly reveals the nanocrystalline nature of the compound. The experimental line profile was fitted for seven peaks (220), (311), (400), (105), (312), (511), and (440) as can be seen in the figure. The average crystallite size, D_{XRD}, of the product was calculated to be 26 ± 4 nm. [12,13].

3.2 FT-IR Analysis

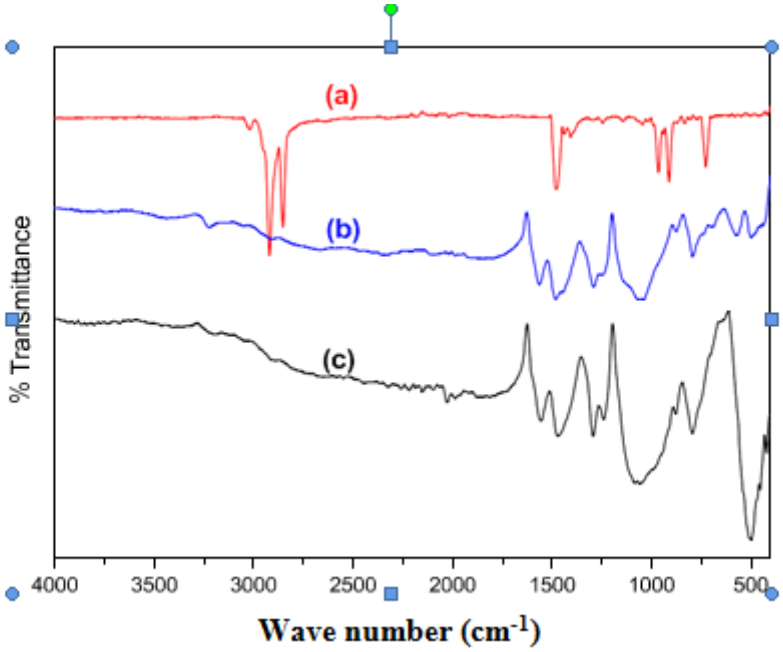

Fig.2: FT-IR spectra of (a) CTAB, (b) PANI and (c) PANI– MnFe2O4-CTAB nanocomposite.

The FT-IR spectra of the three components, PANI–MnFe2O4-CTAB nanocomposite, CTAB, and PANI were presented in Fig. 2a, b, and c, respectively. The symmetric and asymmetric C– H scissoring vibrations of a CH3–N+ moiety between pure CTAB molecules (1482, 1430 cm−1) (Fig. 2a) was also observed in the FT-IR spectra of nanocomposite (Fig. 2c).The peaks at 1564 and 1488cm−1 are attributed to the characteristic C=C stretching of the quinoid and benzenoid rings, the peaks at 1303 and 1246 cm−1 are assigned to C–N stretching of the benzenoid ring, the broad peak at 1143 cm−1.The peak at around 566cm−1 is believed to be for a strong M–O absorption band [18,24].

3.3 TEM Analysis ℃

The Morphological structure of PANI–$MnFe_2O_4$-CTAB nanocomposite was fully investigated by TEM and few micrographs are taken at various magnifications as can be seen Fig. 3. The magnetic particle, $MnFe_2O_4$ was observed to have a mixture of near spherical and polygonic morphology with particles having sizes in the range of 10 and 150 nm. The particles are visible in the micrographs, which directly affect the magnetic properties of the nanoparticles [16,17].

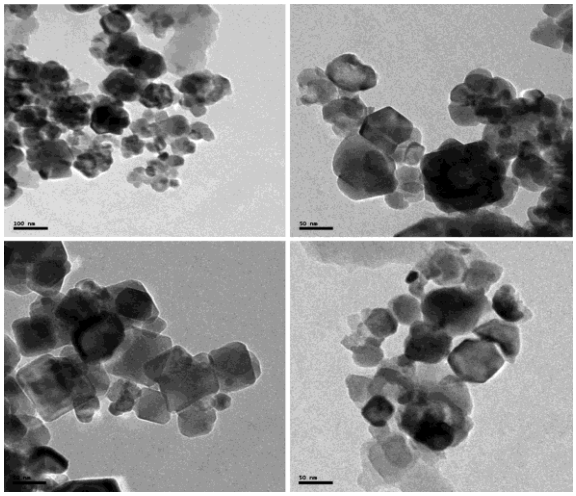

Fig.3:TEM Images of PANI-MnFe2O4-CTAB nanocompound with different magnification

3.4 VSM Analysis

Fig.4 revealed the dependence of the magnetization on the field (hysteresis loops) in the magnetic field range of ±3.5 kOe and in the temperature range of 10–400 K for the PANI–$MnFe_2O_4$–CTAB nanocomposite. It can be observed that the magnetization curves show hysteretic behaviour, indicating that the PANI–$MnFe_2O_4$– CTAB nanocomposite in RTILs has ferromagnetic order in the temperature range of 10–400 K. Also, the hysteretic behavior at 400 K shows the blocking temperature (T_B) to be above 400 K. The observed hysteresis loops are char- acterized by nonsaturated magnetization behavior even up to the applied field of 50 kOe, suggesting to the existence of antiferromagnetic interactions [21, 22]. Similar observations have been reported by R. Topkaya et al. and H. Sozeri et al. [19, 23].

The observed nonsaturated magnetization behavior indicates the presence of disordered spins in the surface of the PANI–$MnFe_2O_4$–CTAB nanocomposite in RTILs [20,24]. The reduced coordination and broken exchange bonds between surfaces spins bring about the disordered surface spins in the magnetic nanoparticles [21,25].

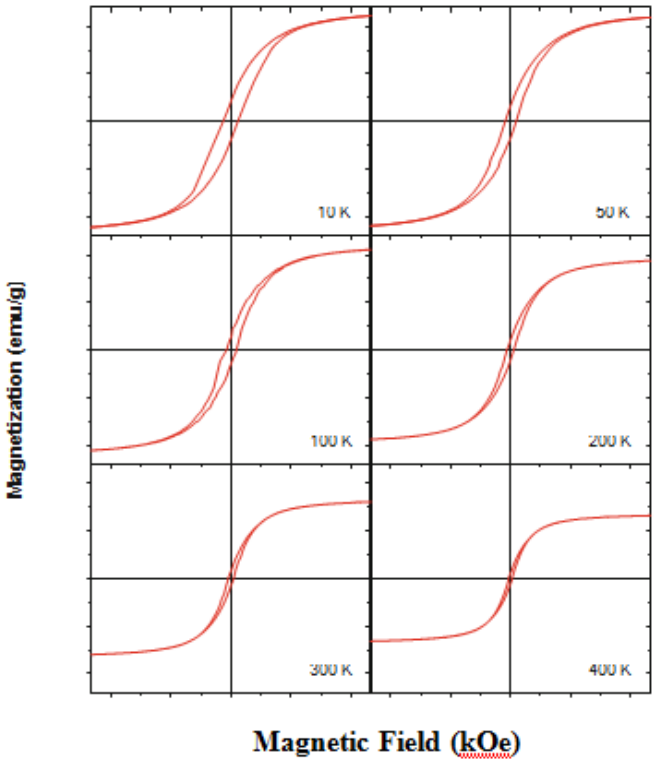

Fig.2: Hysteresis loops of PANI-$MnFe_2O_4$-CTAB nanocomposite at different temperatures

Fig. 5 shows the temperature dependence of the saturation magnetization, Ms for the PANI–$MnFe_2O_4$–CTAB nanocomposite in RTILs. The saturation magnetization values are obtained from the intercept of the magnetization axis as 1/H approaches zero. Ms decreases with increasing temperature, as could be expected by increasing the temperature, the weakening of the exchange interactions between tetrahedral sites (A sites) and octahedral sites (B sites) leads to decrease in Ms [26]. Ms values are lower compared to bulk value of the $MnFe_2O_4$ [22, 27]. The lower Ms value of the magnetic nanoparticles is attributed to the nonmagnetic coating layer by poly aniline polymer and CTAB this is because the coating of the nanoparticles with nonmagnetic chemical materials like polymers weak the magnetic dipole–dipole interactions between neighboring particles and thus total magnetic moment decreases.

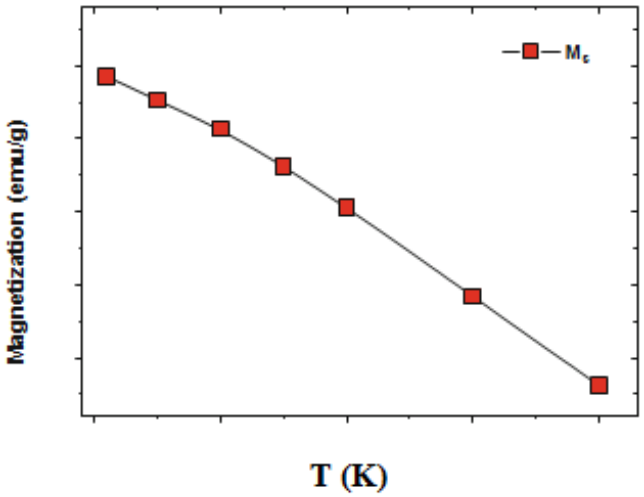

Fig. 5: Temperature dependence of the saturation magnetization (*Ms*) for PANI-$MnFe_2O_4$-CTAB.

The temperature dependence of the coercive field H_c of the PANI–$MnFe_2O_4$–CTAB nanocomposite in RTILs is shown in Fig. 6. H_c continually increases with decrease in temperature, as expected [14]. It is well known that thecoercivity is associated with the magnetocrystalline anisotropy [15]. The increase in H_c is attributed to increase of the effective magnetic anisotropy, K_{eff} with decreasing temperature [24].

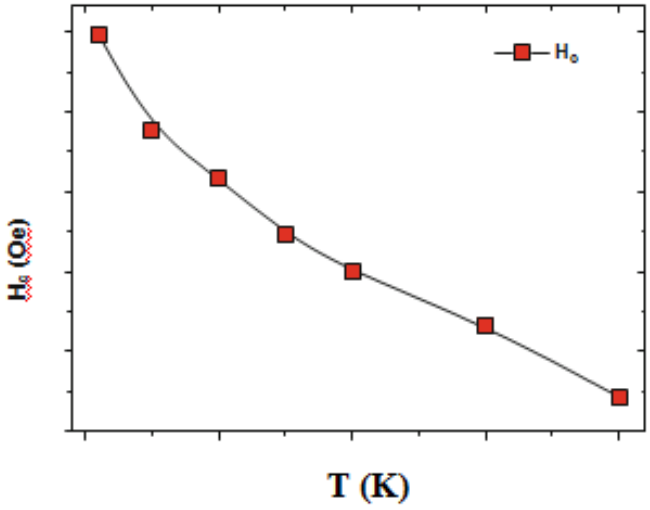

Fig. 6: Coercive field H_c as a function of temperature for PANI-$MnFe_2O_4$–CTAB nanocomposite in RTILs

3.5 TG Analysis

Fig. 7 represents the TG thermogram of the product, which displays three weight loss processes. The first weight loss should be due to the dehydration of the samples (humidity) (between 25 and 200 °C) [10], the second and third weight losses were observed between 210 and 750 °C corresponds to the desorption and subsequent evaporation of organic layer (PANI, CTAB and RTILs). Above 750 °C, product does not present any weight loss due to the presence of only $MnFe_2O_4$ nanoparticles. Therefore, TG analysis showed that weight percentage of organic (including water also) and inorganic layer in the product are 47 and 53 respectively.

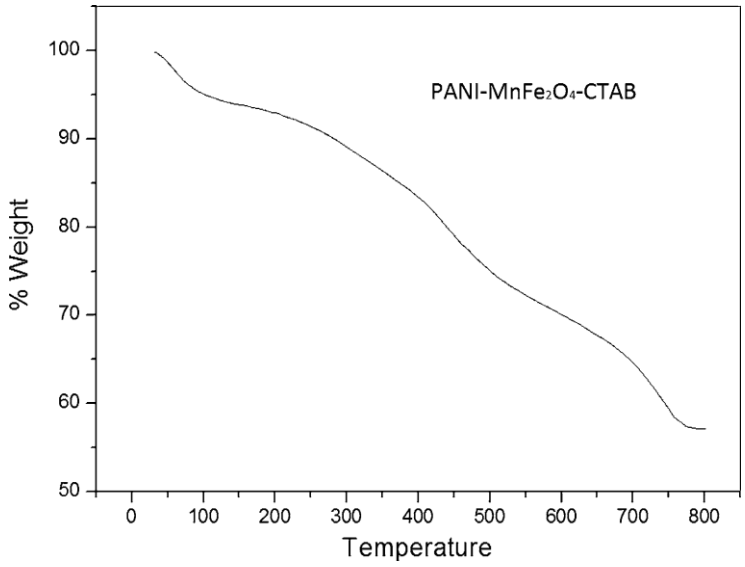

Fig. 7: TG thermogram of PANI–$MnFe_2O_4$–CTAB nanocomposite in RTILs

3.6 Electrical and permittivity properties

The conductivity and permittivity of PANI–$MnFe_2O_4$- CTAB nanocomposite in RTILs were quantified after two electrode connections were used for measuring under different conditions temperatures ranging from 20 to 120 ^oC in a frequency of up to 3 MHz. The ac conductivities of samples used in this study are represented in Fig. 8. It is seen clearly that conductivity in general remains almost unchanged until it reaches up to 160 kHz, and then reduces slightly almost for temperature over 50 ^oC, except for tremendous fluctuations which is observed at lower temperatures. Conductivity varies between 1.15–1.55 mS/cm at all temperatures for all frequencies ranges interested.

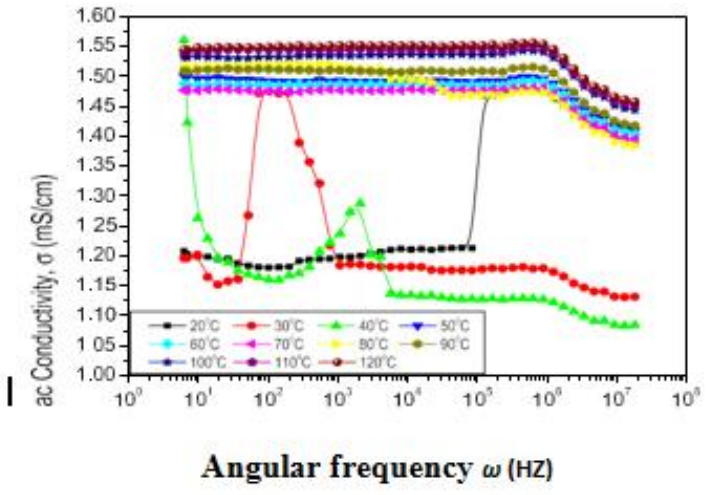

Fig. 8: Plot of ac conductivity of PANI-$MnFe_2O_4$-CTAB nanocomposite in RTILs at different temperature ranging from 20 to 120 ^oC from frequency range of up to 3 MHz.

The dc conductivity of PANI–$MnFe_2O_4$-CTAB nanocomposite in RTILs in the form of Arrhenius plots is shown in Fig. 9 together with two activation energies. The activation energies extracted from a linear fitting at two temperature ranges are given with values of 10 μeV and 1.23 meV obeying a standard exponential decay form as expected. This can be followed by a standard correlation of activation energy as shown in the following Arrhenius formula:

$$\delta \text{ dc (T)} = \delta(0)\ exp - \frac{Ea}{kT} \qquad \text{Eqn. 1}$$

In accordance with Arrhenius plots (Eqn. 1), the activation energy is best regarded as an experimentally resolved parameter that reveals the sensitivity of the reaction rate to temperature [6]. It shows that ac conductivity almost unchanged with frequency up to 3.0 MHz as mentioned earlier, although, initially fluctuates at lower temperatures, and slightly increases with temperatures up to 120 ^oC (Fig. 8). However, this type of characteristic

performance confirms that conductivity is irrelevant to hopping-style conduction, but controlled by temperature-assisted conduction mechanisms being more predominance in this manner.

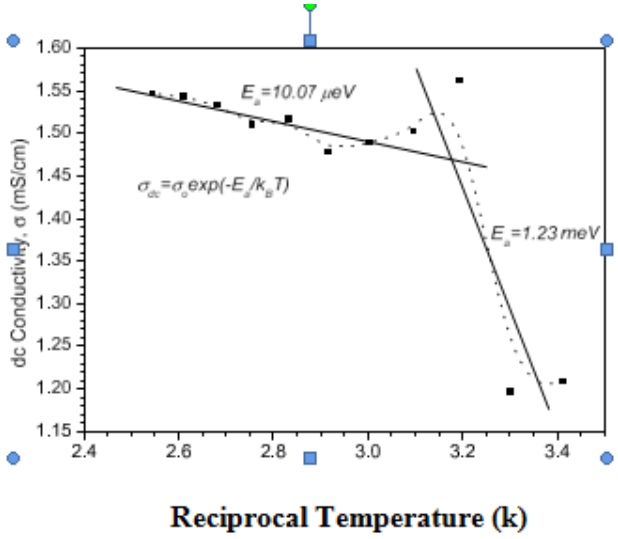

Fig. 9: Plot of dc conductivity against reciprocal temperature together with activation energies of the compound.

Real components of permittivity of the nanocomposite synthesized in RTILs is represented in Fig. 10 as a function of frequency of up to 3MHz for temperature ranging from 20 to 120 ºC. From the figure it can be seen that the real permittivity fluctuates at lower frequencies but independent of temperature at medium and higher frequencies.

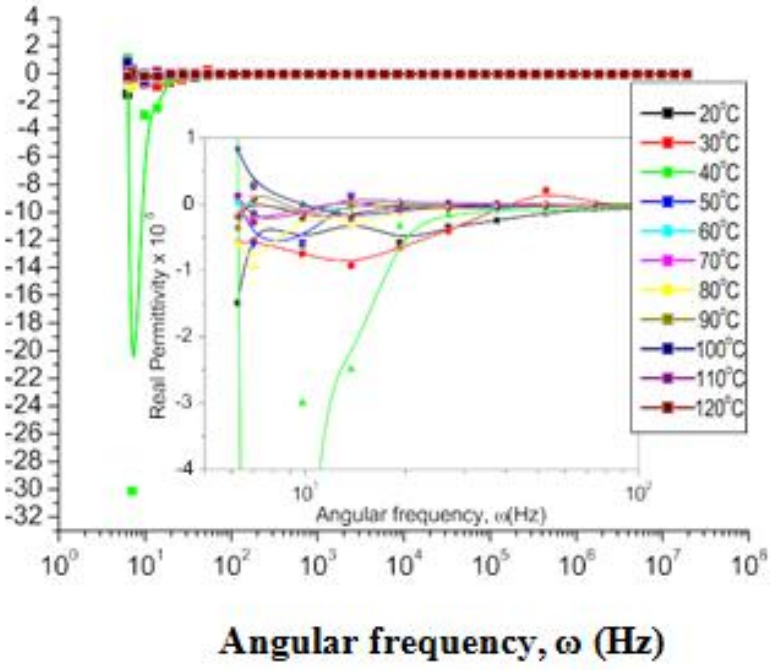

Fig.10: Plot of real component of permittivity against angular frequency of PANI-$MnFe_2O_4$-CTAB nanocomposite in RTILs.

4. CONCLUSIONS

PANI-$MnFe_2O_4$-CTAB was fully synthesized in present RTILs which were generally characterized to have temperature dependence on conduction mechanism (dielectric behavior and electrical properties). The ac conductivity plot also revealed that it almost remains unchanged until around temperature of 120 ºC, which proved that the characteristic performance of conductivity is irrelevant to hopping type conduction which is independent on frequency.

ACKNOWLEDGMENTS

The authors appreciate the funding of this research from Tertiary Education Trust Fund (TETFund), Ministry of Education, the Federal Republic of Nigeria (through Kano University of Science and Technology, Wudil), under Institutional Based Research (IBR) grant with project number (TETFUND/DR&D/UNI/WUDIL/RG/2018/VOL.I).

References

1. Lucigno, C., Quadrini, F., Santo, L.: J. Compos. Mater. **42**, 2841 (2008)
2. Hussain, F., Hojjati, M., Okamoto, M., Gorga, R.E.: J. Compos. Mater. **40**, 1511 (2006)
3. Nguyen, V.H., Haldorai, Y., Phama, Q.L., Shim, J.J.: Mater. Sci. Eng. B **176**, 773 (2011)
4. Karaog˘lu, E., Baykal, A., Deligöz, H., S¸enel, M., Sözeri, H., Toprak, M.S.: J. Alloys Compd. **509**, 8460 (2011)
5. Yang, H., Zhang, C., Shi, X., Hu, H., Du, X., Fang, Y., Ma, Y., Wu, H., Yang, S.: Biomaterials **31**, 3667 (2010)
6. Sun, C., Lee, J.: Adv. Drug Deliv. Rev. **60**, 1252 (2008)
7. Nguyen, V.H., Haldorai, Y., Phama, Q.L., Shim, J.J.: Mater. Sci. Eng. B **176**, 773 (2011)
8. Goldman, A.: Modern Ferrite Technology. Van Nostrand– Reinhold, New York (1990)
9. Kitamoto, Y., Kantake, S., Shirasaki, S., Abe, F., Naoe, M.: J. Appl. Phys. **85**, 4708 (1999)
10. Shuping,Y.,Mingjun,Xi.,Kefei,H.,Zhongming,W.,Wensheng,Y., Hong, Z.: Thin Solid Films **519**, 357 (2010)
11. Jing,L.,Lihua,Z.,Yinghui,W.,Yutaka,H.,Aiqing,Z.,Heqing,T.:Polymer**47**,7361(2006)
12. Yakuphanoglu,F.,Basaran,E.,Senkal,B.F.,Sezer,E.:J.Phys.Chem.B**110**, 16908(2006)
13. MacDiarmid,A.G.,Chiang,J.C.,Richter,A.F.,Epstein,A.J.:Synth.Met.**18**, 285(1987)
14. Elizabeth,W.P.,Antonio,J.R.,Wrighton,M.S.:J.Phys.Chem.**89**,1441(1985)
15. Guo,Y.,Zhang,Y.,Liu,H.,Lai,S.W.,Li,Y.,Li,Yu.,Hu,Wo.,Wang,S.,Che,C.M.,Zhu,D.:J.Phys.Chem.Lett.**1**,327(2010)
16. Bereznev,S.,Kois,J.,Golovtsov,I.,Opik,A.,Mellikov,E.:ThinSolidFilms**511–512**,425 (2006)
17. Heeger,A.J.,long,J.:Opt.PhotonicsNews**7**,24(1996)
18. Yu,G.,Gao,J.,Hummelen, J.C.,Wudl,F.,Heeger, A.J.:Science **270**,1789(1995)
19. Baykal,A.,Kasapog˘lu,N.,Köseog˘lu,Y.,Toprak,M.S.,Bayrak- dar,H.:J.AlloysCompd.**464**,514(2008)
20. M.Gu¨nay,H.Erdemi,A.Baykal,H.So¨zeri,M.S.Toprak,Mater. Res.Bull.48,1057(2013)
21. R.Topkaya,O¨.Akman,S.Kazan,B.Aktas¸, Z.Durmus,A. Baykal,J.Nanopart.Res.14,1156(2012)
22. K.K.Bharathi,R.J.Tackett,C.E.Botez,C.V.Ramana,J.Appl.Phys.109,07A510(2011)
23. H.Sozeri,U.Kurtan,R.Topkaya,A.Baykal,M.S.Toprak,Ceram.Int.39,5137(2013)
24. K.Parekh,R.V.Upadhyay,J.Appl.Phys.107,053907(2010)
25. R.H.Kodama,A.E.Berkowitz,E.J.JrMcNiff,S.Foner,Phys.Rev.Lett.77,394(1996)
26. Z.H.Zhou,J.M.Xue,H.S.O.Chan,J.Wang,J.Appl.Phys.90,4169(2001)